RSC Advances

PAPER

View Article Online
View Journal | View Issue

Cite this: *RSC Adv.*, 2024, **14**, 30385

Synthesis and photophysical properties of novel bis-quinolin-3-yl-chalcones†

Indhu Chandrasekaran and S. Sarveswari *

A novel series of unsymmetrical bis-quinolin-3-yl chalcones has been synthesized under visible light using a Claisen–Schmidt condensation reaction between the 2-(morpholine-piperidine-pyrrolidine-thiomorpholine) substituted quinoline-3-carbaldehyde and 1-(2-methyl-4-phenylquinolin-3-yl) ethan-1-one derivatives, conducted at room temperature in the presence of NaOH/EtOH. The structures of the synthesized compounds have been confirmed by NMR spectroscopy and high-resolution mass spectroscopy. The synthesized compounds exhibit λ_{max} values ranging from 215 nm to 290 nm in non-polar to polar solvents, demonstrating positive solvatochromism. Compounds containing nitro group substituent exhibit a significant blue shift owing to their strong electron-withdrawing ability, which also contributes to fluorescence quenching. Geometrical optimization and the calculation of HOMO, LUMO, and energy gap are calculated by using the DFT/B3LYP/6-31G(d) method.

Received 13th June 2024
Accepted 11th September 2024

DOI: 10.1039/d4ra04335a

rsc.li/rsc-advances

1. Introduction

Chalcones are α,β-unsaturated ketones that are naturally distributed in a diverse range of plants, fruits, and vegetables. They serve as important precursors in flavonoid and isoflavonoid synthesis,[1,2] contributing significantly to the yellow pigmentation observed in various plant organs.[3] Structurally, chalcones consist of two aromatic rings interconnected by a ketoethylenic chain.[4] The two aromatic rings in the chalcones often constitute a donor–acceptor–donor (D–A–D) core and generally undergo intramolecular charge transfer (ICT).[5] The alteration in its photophysical activity can be achieved by modulating the electron donors or acceptors within the core structure. Beyond their extensive biological applications,[6–9] they also act as photoinitiators,[10] photosensitizers,[11] sensors,[12,13] fluorescent dyes,[14] fluorescent probes,[15] optoelectronic devices,[16] and nonlinear optical materials.[17,18] They also serve as a precursor for various heterocyclic compounds through ring closure reactions.[19,20]

A plethora of synthetic methods have been reported for chalcone synthesis because of their simplicity of structure, ease of construction, and promising biological activities.[21] Several pathways such as Claisen–Schmidt condensation, Carbonylative Heck's coupling reaction, Suzuki–Miyaura's coupling reaction, and Sonogashira's isomerization coupling[22] have been employed for the process. But the Claisen–Schmidt condensation is carried out in basic or acidic media under homogeneous conditions[23] remains a conventional method. Though it bears several drawbacks such as slow reaction rate, the formation of by-products, and incomplete reaction yet regardless of this it is the most common and simple procedure with enhanced yield as compared to other common methods.[24] Traditional Claisen–Schmidt reaction has been performed by using aqueous NaOH or KOH or ethanolic NaOEt at 50 °C over a time of few to several hours.[25] It has certain inherent limitations, such as prolonged reaction times, reported lower yield, and a requirement of high temperatures, for example, the Tiwari V.[26] (Scheme 1), Desai N. C.,[27] and Peerzade N.[28] reported the chalcone synthesis in good yield but the reaction duration was about 24 hours. In contrast, Kachadourian R., and Cho C. (Scheme 1), were able to shorten the reaction[29,30] duration by elevating the temperature (up to 80 °C), underscoring the role of temperature in accelerating chalcone synthesis and potentially facilitating faster reaction. There are numerous reports utilising microwave irradiation,[31–34] sonication,[35–37] and conventional reflux methods for this purpose. Although, ultrasonication[38] and microwave

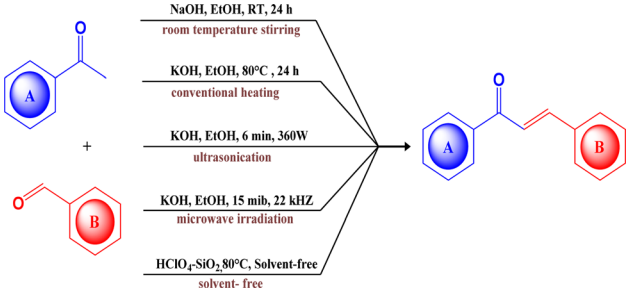

Scheme 1 Different approaches for the synthesis of chalcone derivatives of quinoline.

Department of Chemistry, School of Advanced Sciences, VIT University, Vellore 632014, Tamil Nadu, India. E-mail: ssarveswari@vit.ac.in

† Electronic supplementary information (ESI) available. See DOI: https://doi.org/10.1039/d4ra04335a

irradiation[39] (Scheme 1) have also positively impacted the reaction duration and the total yield, it requires a comparatively complex setup.

Thus, our curiosity led us to investigate visible light irradiation in the Claisen–Schmidt condensation as an alternative energy source to enhance yields at room temperature with a simpler setup. Visible light irradiation introduces an innovative aspect to the traditional Claisen–Schmidt condensation, providing a mild and sustainable energy source that facilitates the reaction through photochemical pathways. As visible light represents a renewable, clean, and abundant energy source,[40] this approach harnesses enough energy to perform the reaction without the disadvantages of thermal activation, such as high temperatures or harsh reaction conditions.[41] Recent advances in visible-light-driven organic reactions have attracted extensive attention from the synthetic community.[42] It also offers numerous applications, such as mild reaction conditions,[43] minimal side reactions,[44] simple experimental setups,[45] and increased product yields. Under visible light irradiation, electrons can be excited from the ground state to higher-energy orbitals when the incident light energy matches the electronic transition energies in molecules. Electron transitions can occur from the highest occupied molecular orbital (HOMO) to the lowest unoccupied molecular orbital (LUMO). The photoexcited electrons then return to the ground state through electron-vibration coupling, generating heat within the molecules.[46,47] Accordingly, we endeavoured to synthesize a novel series of unsymmetrical bis-quinolin-3-yl chalcones (Fig. 1) under visible light. This synthesis involved the incorporation of two crucial groups of quinoline derivatives in terms of application, such as yield 2-(morpholine-piperidine-pyrrolidine-thiomorpholine) substituted quinoline-3-carbaldehyde (**3–6**) and derivatives of quinoline (**12–16**). Notably, while quinolinyl chalcones are frequently reported in the literature, reports on bis-quinolin-3-yl chalcones are scarce, with only a few instances documented.[48,49]

The utilisation of visible light has been positively reflected in both the reaction kinetics and product yield during the present synthesis of bis-quinolin-3-yl chalcones. Thus, a novel series of chalcones were synthesized with improved yield, and shorter reaction duration, without the use of any harsh conditions or reagents. The synthesised compounds were confirmed using spectral techniques, and photophysical investigations were conducted to assess the influence of solvents and substituents. Density Functional Theory (DFT) calculations were also carried out for geometry optimisation and the determination of frontier molecular orbitals. Various global parameters, including Highest Occupied Molecular Orbital (HOMO), Lowest Unoccupied Molecular Orbital (LUMO), energy gap, ionisation potential, hardness, softness, electronegativity, and electrophilicity index were also calculated to elucidate the electronic properties of the synthesised chalcones.

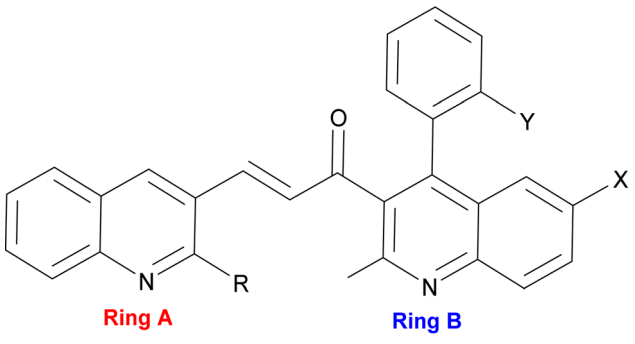

General structure

Fig. 1 The general structure of the synthesized unsymmetrical bis-quinolin-3-yl chalcones.

2. Results and discussion

2.1 Chemistry

The precursor necessary for the synthesis, 2-chloro quinoline-3-carbaldehyde (**2**), was synthesised *via* Vilsmeier–Haack reaction[50–53] of acetanilide. Subsequently, it underwent nucleophilic substitution with some secondary amines (*R*-morpholine, piperidine, pyrrolidine, or thiomorpholine) to yield 2-(morpholine-piperidine-pyrrolidine-thiomorpholine) substituted quinoline-3-carbaldehyde (**3–6**).[54,55] The synthesis of another precursor involved Friedlander cyclization to obtain derivatives of quinoline (**12–16**) from the corresponding substituted 2-aminobenzophenones (**7–11**) (where X–Cl, H or NO_2 and Y– Cl, H, and F) and acetylacetone in an acidic medium (HCl)[56–58] as depicted in Scheme 2.

Unsymmetrical bis-quinolin-3-yl chalcones (**17–36**), were synthesized through Claisen–Schimdt condensation of the aforementioned 2-(morpholine-piperidine-pyrrolidine-thiomorpholine) substituted quinoline-3-carbaldehyde (**3–6**), and derivatives of quinoline (**12–16**) with ethanol as solvent. Initially, optimisation of the reaction was performed using the model reaction of 1-(6-chloro-2-methyl-4-phenylquinolin-3-yl) ethan-1-one (**12**), and 2-morpholinoquinoline-3-carbaldehyde (**3**) under various conditions (refer to Table 1), including different bases such as NaOH, KOH, K_2CO_3, and pyridine, under an air atmosphere at room temperature. The progress of the reaction was monitored using Thin Layer Chromatography (TLC), demonstrating the formation of the reaction of the desired product (**17**), with a better yield of 65% in NaOH. The screening of different bases revealed the initially used NaOH was the best.

Conversely, the model reaction was conducted under the absence of light and in visible light irradiation to investigate the impact of various sources of visible light on the Claisen–Schmidt condensation. Initially, without any base, no product formation was observed even after 24 hours. Following this, we reintroduced the optimized base, NaOH, into the reaction. Firstly, to optimize the role of the light in this reaction, the reaction was carried out using NaOH as the catalyst in the absence of light, the yield of the desired product was lower, similar to that of entry 1 of Table 1, achieving only 63% at the end of 8 hours. On the other hand, when the model reaction was subjected to various visible light irradiation with the same condition, the one with blue LED irradiation, showed the formation of the desired product with a yield of 92% at the end

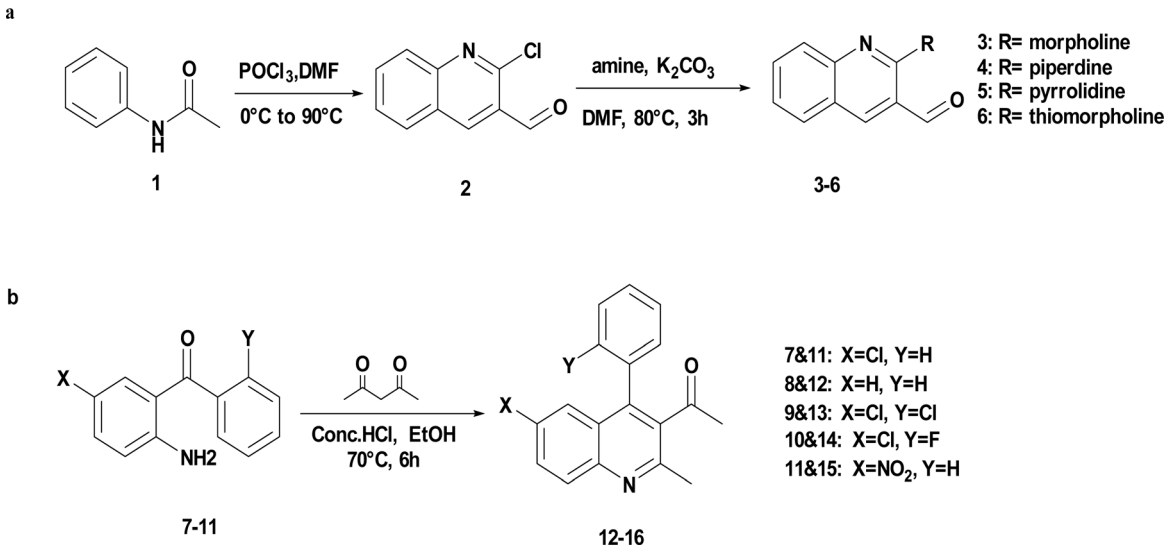

Scheme 2 (a) Substrate scope of 2-(morpholine-piperidine-pyrrolidine-thiomorpholine) substituted quinoline-3-carbaldehyde (**3–6**). Reaction conditions: (**2**) (1 mmol), secondary amine (2 mmol), K_2CO_3 (2 mmol). DMF (10 mL), 6 80 °C, 3 h (b) substrate scope of derivatives of quinoline (**12–16**). Reaction conditions: (**7–11**) (1 mmol), acetylacetone (4 mmol), EtOH (10 mL), and conc. HCl, 70 °C, 6 h.

Table 1 Optimisation of the reaction conditions[a]

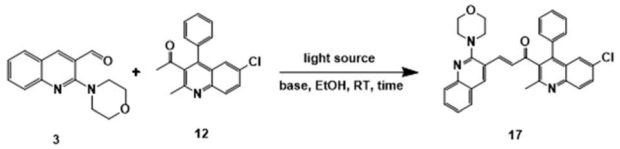

Entry	Base	Light source	Time	Yield[b] (%)
1	NaOH	—	16	65
2	KOH	—	20	55
3	K_2CO_3	—	18	62
4	Pyridine	—	17	60
5	—	Dark	24	—
6	—	Green LED	24	—
7	—	Blue LED	24	—
8	—	Red LED	24	—
9	NaOH	Dark	8	63
10	NaOH	Green LED	8	78
11	**NaOH**	**Blue LED**	**8**	**92**
12	NaOH	Red LED	8	70

[a] Unless otherwise reported, reaction was performed with 3 (1 mmol), 12 (1 mmol), ethanol (10 mL), room temperature. [b] isolated yields.

of 6 hours. This observation reveals that use of a blue LED notably improved the yield to 92%. This significant improvement suggests that visible light enhances yield and reduces the reaction duration by providing the necessary energy for the reaction, overcoming the thermal limitations of conventional heating. The role of light here is analogous to that of any thermal source, enhancing the reaction kinetics by effectively exciting the molecules.

To further validate the practicality of this methodology, a scale-up reaction was performed on a 10 mmol scale. This larger-scale reaction proceeded smoothly under optimized conditions, highlighting the synthetic advantages of this protocol. While we have aimed to achieve shorter reaction durations similar to those obtained with ultrasonication and microwave irradiation, we successfully achieved a comparatively shorter reaction duration than with conventional methods. These findings underscore the potential of visible light as an efficient alternative energy source for driving chemical reactions, offering a green and effective approach to enhancing reaction yields and reducing times.

With the established optimal reaction conditions, a range of unsymmetrical bis-quinolin-3-yl chalcones (**17–36**) (Scheme 3) was synthesised, yielding high to excellent yields exceeding 85%. This protocol avoids the necessity for elevated temperatures, metal catalysts, ultrasound, or microwave irradiation. All the compounds involved filtration of the reaction mixture, followed by pouring into cold water. Subsequently, crude products were purified *via* column chromatography. Based on the obtained results and existing literature precedents, even though its specific reaction mechanism is not yet apparent, a plausible mechanism may involve promotion of reaction in the presence of visible light by exciting the electrons in the reactants. This excitation can lower the activation energy of the reaction steps, particularly the enolate formation and the nucleophilic attack. Visible light photons are absorbed by the reactants, causing the excitation of π-electrons to higher energy states. The excited state of the carbonyl compounds (both aldehyde and ketone) can have altered electronic distributions, increasing their reactivity towards nucleophilic attack and base catalysis. Then, the base (OH^-) can more readily deprotonate the excited ketone, forming the enolate more efficiently. This enol form is highly reactive and readily undergoes subsequent reactions. The enol form of acetophenone reacts with 2-(morpholine-piperidine-pyrrolidine-thiomorpholine) substituted quinoline-

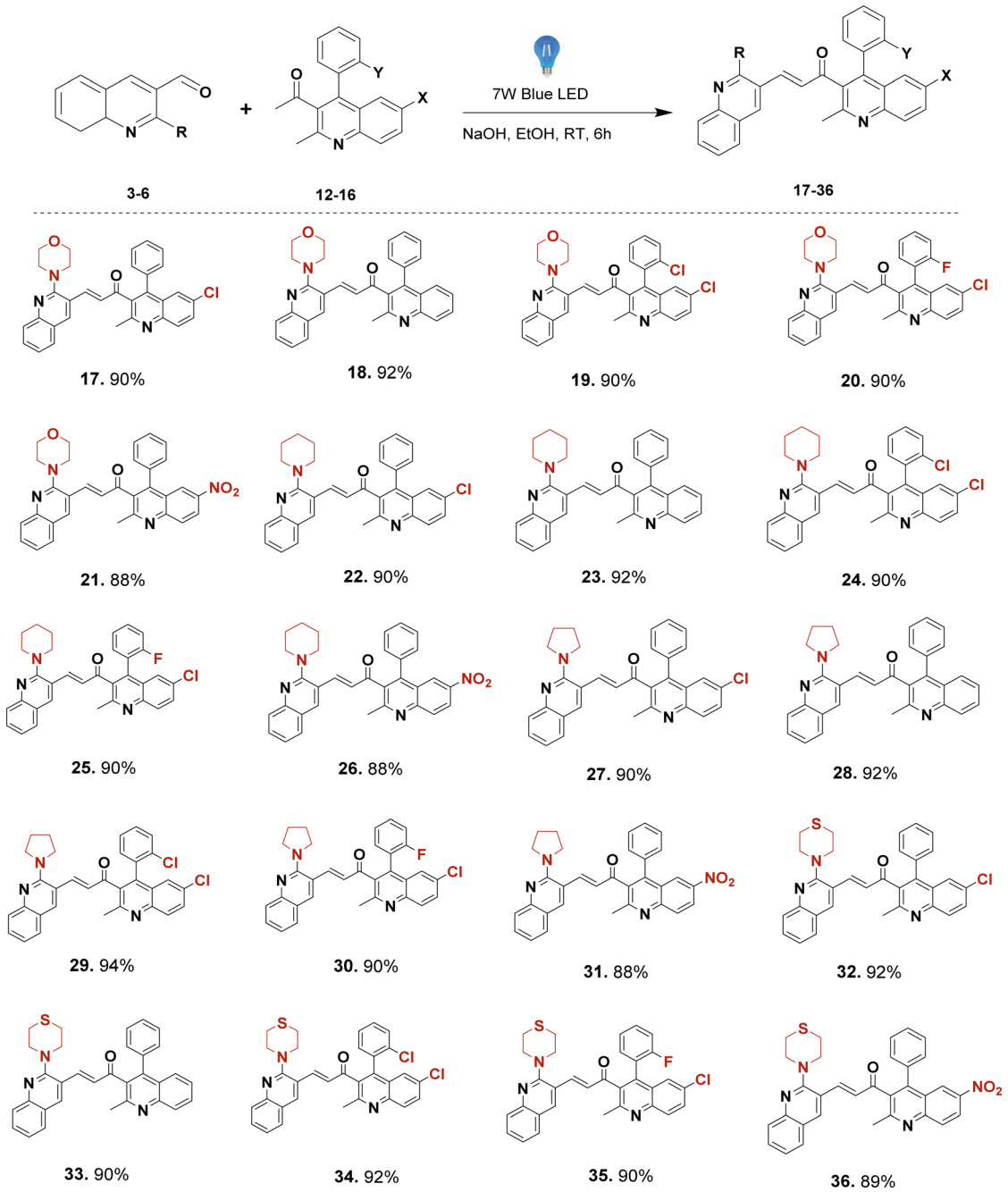

Scheme 3 Substrate scope of bis-quinolin-3-yl chalcones (**17–36**). Reaction conditions: compounds (**3–6**) (1 mmol, 1 eq.) and compounds (**12–16**) (1 mmol, 1 eq.), EtOH (10 mL), NaOH, room temperature, 6 h, under visible light (7 W Blue LED) radiation. Isolated yields.

3-carbaldehyde *via* an aldol condensation reaction. The enol attacks the carbonyl carbon of the aldehyde, forming an unstable intermediate. The intermediate formed undergoes dehydration, leading to the formation of a carbon–carbon double bond between the α and β carbons, resulting in the formation of the chalcone. Overall, the visible light provides the energy needed to initiate the photoenolization of acetophenone, which then undergoes subsequent reactions to form the chalcone product. This mechanism allows for the synthesis of chalcones under milder conditions compared to traditional thermal methods.

2.2 Photophysical study

2.2.1 Absorption and emission spectroscopic study. The absorption and emission spectra of the synthesized compounds (**17–36**) were initially recorded in acetonitrile, a highly polar aprotic organic solvent (where the photolysis is reduced due to lack of water), and the corresponding photophysical data are summarised in Table 2. As illustrated in Fig. 2, the absorption spectra of all compounds exhibit an intense sharp band (λ_{max}) around the region of 262 to 277 nm and a secondary, less intense broader band around the region of 310–330 nm. The

Table 2 Global reactivity parameters of all the synthesised compounds

Compounds	E_{HOMO} (eV)	E_{LUMO} (eV)	Ionisation potential, $I = -E_{HOMO}$ (eV)	Electron affinity, $A = -E_{LUMO}$ (eV)	Hardness $\eta = (I - E)/2$ (eV)	Softness, $\sigma = 1/2\eta$ (eV)	Electro negativity, $\chi = (I + E)/2$ (eV)	Electrophilicity index, $\omega = \mu^2/2\eta$ (eV)	Energy band gap, $\Delta E = \lvert E_{HOMO} - E_{LUMO} \rvert$ (eV)
17	−5.3933	−2.3211	5.3932	2.3211	1.5360	0.3255	3.8572	4.8428	3.07
18	−5.3796	−2.3211	5.3796	2.3211	1.5292	0.3269	3.8504	4.8472	3.0585
19	−5.4722	−2.5252	5.4722	2.5252	1.4734	0.3393	3.9987	5.4257	2.9469
20	−5.4967	−2.3565	5.4967	2.3565	1.5700	0.3184	3.9266	4.9099	3.1401
21	−5.5728	−2.3673	5.5728	2.3673	1.6027	0.3119	3.9701	4.9171	3.2055
22	−5.4177	−2.1905	5.4177	2.1905	1.6136	0.3098	3.8041	4.4841	3.2272
23	−5.3660	−2.1170	5.3660	2.1170	1.6245	0.3077	3.7415	4.3087	3.2490
24	−5.4994	−2.2585	5.4994	2.2585	1.6204	0.3085	3.8789	4.6427	3.2408
25	−5.4967	−2.3565	5.4967	2.3565	1.5700	0.3184	3.9266	4.9099	3.1401
26	−5.5837	−3.4123	5.5837	3.4123	1.0857	0.4605	4.4980	9.3173	2.1714
27	−5.5239	−2.3456	5.5239	2.3456	1.5891	0.3146	3.9347	4.8712	3.1782
28	−5.4477	−2.2204	5.4477	2.2204	1.6136	0.3098	3.8340	4.5549	3.2272
29	−5.5620	−2.4082	5.5620	2.4082	1.5769	0.3170	3.9851	5.0355	3.1538
30	−5.4422	−2.3864	5.4422	2.3864	1.5279	0.3272	3.9143	5.0140	3.0558
31	−5.6137	−3.4123	5.6137	3.4123	1.1007	0.4542	4.5130	9.2519	2.2014
32	−5.6055	−2.3946	5.6055	2.3946	1.6054	0.3114	4.0000	4.9831	3.2109
33	−5.4749	−2.4082	5.4749	2.4082	1.5333	0.3260	3.9415	5.0659	3.0667
34	−5.6871	−2.4680	5.6871	2.4680	1.6095	0.3106	4.0776	5.1651	3.2191
35	−5.6708	−2.4435	5.6708	2.4435	1.6136	0.3098	4.0572	5.1006	3.2272
36	−5.7497	−3.4395	5.7497	3.4395	1.1551	0.4328	4.5946	9.1378	2.3102

Fig. 2 The absorption spectroscopy of all the synthesized compounds.

primary peak at around 260 nm is attributed to the π–π* transition within the molecule, likely arising from the presence of multiple aromatic rings and extended conjugation. The secondary band suggests n–π* transitions due to the intramolecular charge transfer (ICT), supported by the large stokes shift values up to 2.1×10^4 cm^{-1}. The absorption maxima of the compounds follow the order of **33** > **32** > **18** > **17** > **23**, indicating compound **33** possesses the highest absorption maxima at 277 nm. This increased bathochromic shift is attributed to thiomorpholine substitution at the 2nd position of ring A. It is because thiomorpholine is the most electron-rich due to the sulfur atom's electron-rich nature, making it the strongest electron donor among the listed secondary amine substituents. Additionally, the absence of an electron-withdrawing group at the 6′ position of ring B in compound **33** prevents a possible hypsochromic shift as observed in compound **32**, which contains a chlorine atom, an electron-withdrawing group at position 6′ of ring B.

The photophysical properties such as stokes shift, molar extinction coefficient, and quantum yield are calculated and presented in Table 2. Quantum yield for compounds with nitro groups is notably low due to fluorescence quenching. Whereas compounds like **12**, **23**, **28**, and **33** exhibit good quantum yields. Most compounds display stokes shifts exceeding 1.5×10^4 cm^{-1}, indicating vibrational relaxation or thermal energy loss before emission. The fluorescence properties of all the synthesized compounds were measured based on the absorption maxima obtained on UV-visible spectroscopy. The broadened emission peaks suggest strong intermolecular interactions and delocalization of π-electrons among the neighbouring molecules in the solid state 53.[59] All the compounds exhibit unique fluorescence in the visible region, consistent with varied quantum yields ranging from 0.1 to 0.7 in acetonitrile. The obtained emission spectra (Fig. 3) are observed in the range of 527 to 568 nm, with compounds containing nitro groups emitting at shorter wavelengths compared to those without

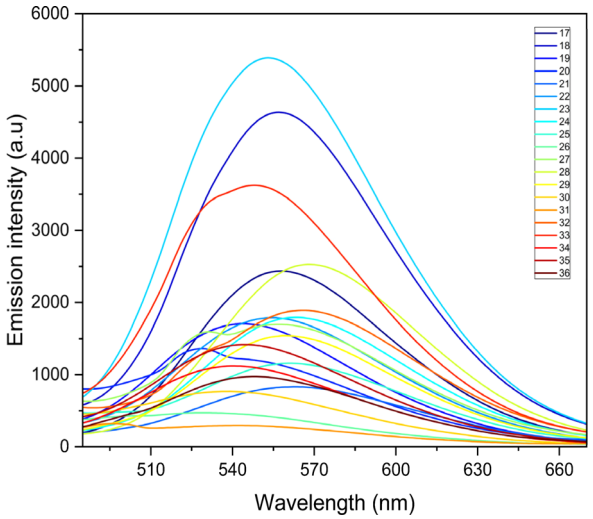

Fig. 3 The emission spectroscopy of all the synthesized compounds.

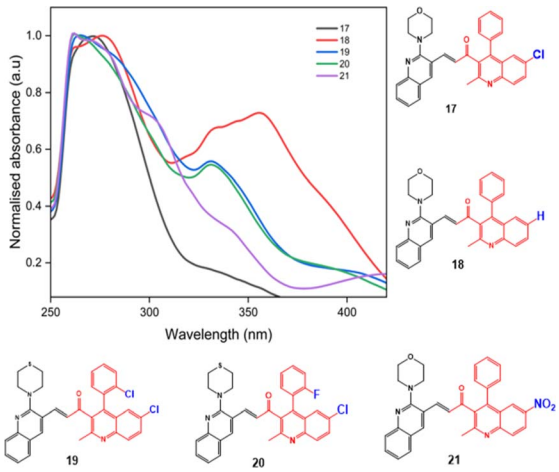

Fig. 5 The substituent effect of compounds **17–21**.

substitution. Also, the introduction of the fluorine atom has a negative effect on the quantum yield as well as the emission intensity, indicating that both nitro groups and halide ions present in the compounds act as quenchers.[60] Also, fluorescence intensities are influenced by substituents and their electron-withdrawing ability. However, bis-quinolin-3yl chalcone derivatives **18**, **23**, and **33** exhibit comparatively high fluorescence intensity.

2.2.2 Solvatochromism. The absorption wavelength of all the synthesized compounds is measured in solvents of varying polarity such as petroleum ether, toluene, diethyl ether, dichloromethane, ethyl acetate, methanol, ethanol, acetonitrile, dimethylformamide, dimethyl sulfoxide. The solvent effect on the absorption spectra of these compounds is depicted in Fig. 4 and the ESI file.† Notably, compound **23** exhibits an absorption wavelength of 215 nm to 290 nm with varying solvent polarities. Analysis of the graph shows a redshift of the π–π* band of the compound as solvent polarity increases, indicating positive solvatochromism. This positive solvatochromism pattern results from the strong interaction of polar solvents with the molecule, stabilising its excited state of the compound and reducing the energy required for excitation. Consequently, the energy difference between the ground state and the excited state decreases, resulting in a red shift in the absorption spectrum.[61]

2.2.3 Substituents effect. The absorbance and emission spectra of all compounds are significantly influenced by the substituents, as demonstrated in Fig. 5 and 6. Thus It is important to investigate the effect of electron-donating and electron-withdrawing groups within these compounds. Initially, the effect of the nitro and halide ions substituted at the 6′ position of ring B was examined through the absorption spectra analysis of compounds **17–21** in acetonitrile, as illustrated in Fig. 5. Analysis of the spectra reveals notable shifts in the λ_{max} values of compounds **17–21**, with observed values of 271 nm for **17**, 277 nm for **18**, 264 nm for **19**, 262 nm for **20**, and 261 nm for **21**, indicating a trend of decreasing absorption maxima as follows: **18** > **17** > **19** > **20** > **21**. Compound **18**, lacking

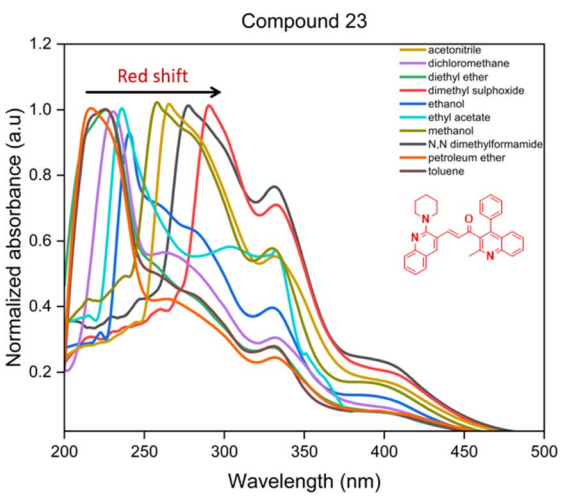

Fig. 4 The solvatochromism of the compound **23**.

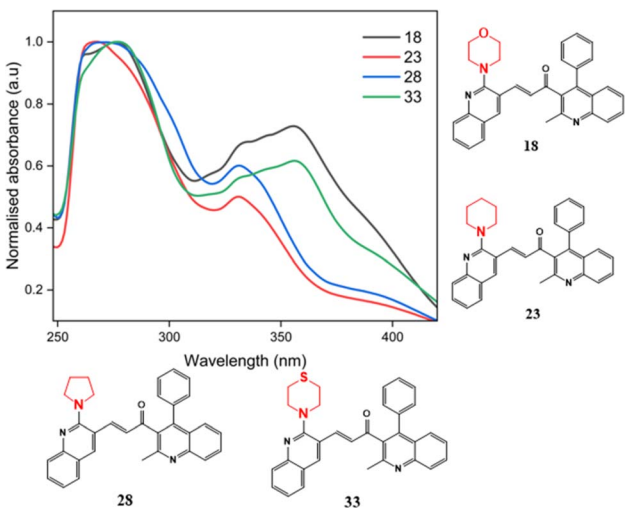

Fig. 6 The substituent effect of the secondary amine substituents.

substitution, exhibits the highest absorption wavelength due to minimal alteration in its electronic structure by hydrogen atoms, thus resulting in relatively high-energy transitions. Compound **17**, featuring chlorine atoms known for their electron-withdrawing effect, experiences a slight blueshift in the absorption spectrum. Compound **19**, with multiple chlorine atoms intensifying the electron-withdrawing effect, demonstrates a more significant blueshift. Compound **20**, featuring fluorine known for its strong electronegativity, further enhances the electron-withdrawing effect, resulting in a pronounced redshift in the absorption spectrum. Nitro groups, highly electron-withdrawing, induce a substantial blueshift in the absorption spectrum, thereby exhibiting the lowest λ_{max} among the compounds. This observation underscores that compounds bearing nitro groups possess lower wavelengths and higher energy levels, rendering them less stable.

Proceeding to investigate the impact of the insertion of secondary amines morpholine, pyrrolidine, piperidine, and thiomorpholine, the absorption maxima of compounds **18**, **23**, **28**, and **33** in acetonitrile solvent as illustrated in Fig. 6. These compounds, lacking substituents at the 6′ position of ring B, are selected to explore the influence of secondary amine substitution on resultant chalcones. From the graph, an evident shift in the λ_{max} value was observed. The recorded values of λ_{max} are 277 nm, 265 nm, 270 nm, and 278 nm for compounds **18**, **23**, **28**, and **33**, respectively. This shift can be attributed to the presence of lone pairs in the sulfur and oxygen atoms of thiomorpholine and morpholine, resulting in comparatively higher wavelengths. Pyrrolidine, a five-membered nitrogen-containing heterocycle, and piperidine, being a basic amine group, displays the shortest wavelength absorption due to its weaker electron-donating effects.

2.3 Computational study

2.3.1 Frontier molecular orbitals. Density functional theory (DFT) computations were performed with B3LYP/631-G(d) method for all the synthesised compounds. The optimised ground state geometries of compounds **23** and **26**, along with frontier molecular orbital (FMO) profiles of the HOMO and LUMO are displayed in Fig. 7 and 8. The optimised geometries reveal non-planar conformations of the compounds. The HOMO and LUMO electronic states are the distribution of the electron cloud within the molecular structure upon excitation. In the case of compound **23**, the HOMOs are predominantly

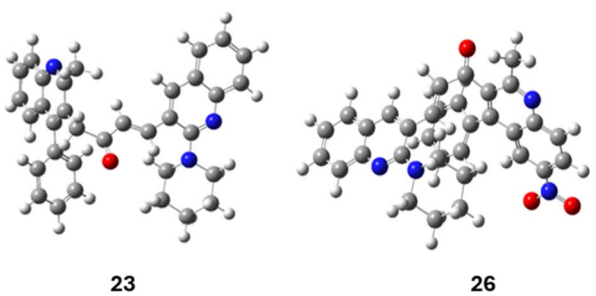

Fig. 7 The optimised geometries of compounds **23** and **26**.

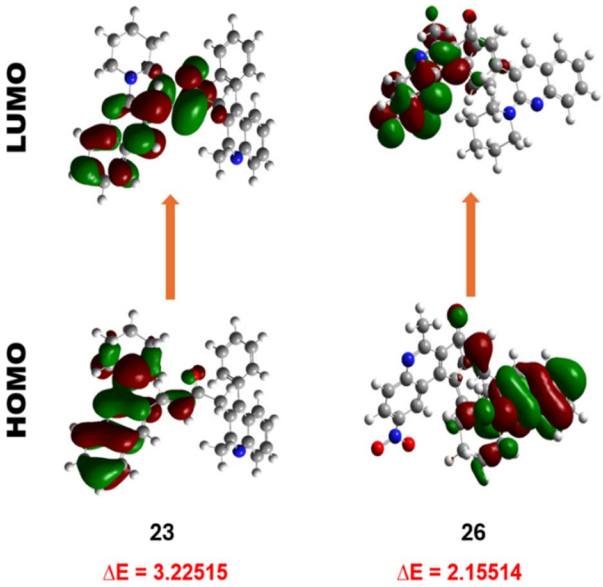

Fig. 8 The frontier molecular orbitals of compound **23** and **26**.

localised over the ring A along with the piperidine ring, with a partial extension over the α,β-unsaturated ketone bond. Upon excitation, electron density from the piperidine ring undergoes delocalisation, shifting entirely towards the α,β-unsaturated ketone bond. The negligible contribution of ring B indicates the minimal role in the charge transfer mechanism. Similar localisation patterns of HOMOs over ring A, are observed across compounds **17–36.**

However, the LUMOs exhibit unique localisation patterns for all the compounds. In most compounds, the LUMO is located all over the molecule except for the substitution at the 2nd position of ring A as observed in compounds **17–20.** However, in compound **26**, the electron density was transferred from the ring A to the ring B upon excitation. This shows the significant interaction between the two quinoline rings. This behaviour is attributed to the presence of a highly electron-withdrawing nitro group substituent in the respective compound, leading to increased intramolecular charge transfer, increased charge separation, and reduced HOMO–LUMO energy band gap compared to the other compounds. The LUMOs of other compounds with nitro group substituents *i.e.*, **21**, **31**, and **36** also exhibit the same localisation pattern and lower energy band gap values. This observation strengthens our interpretation.

2.3.2 Global reactivity parameters. To elucidate the electronic nature of the synthesized molecules, key chemical reactivity metrics, including ionisation potential, electron affinity, electronegativity, global hardness, global softness, electrophilicity index, and energy gap were calculated *via* DFT studies as summarised in Table 2. From the result obtained, compound **23** exhibits the highest energy band gap among all molecules, likely attributed to the absence of a substituent group; thereby reducing conjugation. Consequently, compound **23** displays the highest kinetic stability and correspondingly, the lowest reactivity. Conversely, compound **26** demonstrated the lowest

energy gap, indicating the highest reactivity and diminished stability compared to other compounds. Most of the other parameters show a similar trend consistent with the energy gap trend.

The electron affinity, softness, electronegativity, and electrophilicity index of compound **23** exhibited the lowest values, suggesting it is less prone to undergo charge transfer, affirming its greater stability. Furthermore, compound **26** confirms its greater capacity for energy release, demonstrated by elevated softness, electronegativity, and electrophilicity index value. Compound **36**, featuring a nitro substituent, displayed the highest electron affinity, underscoring the influence of electron-withdrawing groups on stability and being more prone to electron transfer. This observation aligns with the broader trend wherein compounds lacking electron-withdrawing substituents on ring B show enhanced stability. In summary, the DFT calculations provide reasonable insights into the electronic structure of the compounds, supporting the impact of structural variations on stability and reactivity.

3. Experimental

3.1 General information

All the reagents and chemicals utilised were purchased from Sigma-Aldrich and employed without further purification. Melting points were determined by employing the open capillary method. Residual moisture in organic extracts was removed using anhydrous Na_2SO_4. Thin Layer Chromatography (TLC) was conducted on silica gel $60F_{254}$ aluminium sheets. Visualization of spots on TLC plates was achieved through UV light irradiation, iodine exposure, or the application of staining solutions such as KMnO4 and ninhydrin. Crude products underwent purification *via* column chromatography using mesh sizes ranging from 230 to 400. Commercial Blue LEDs rated at 7 W from Crompton were purchased and utilized as such. NMR spectra, including ^1H, ^{13}C, and DEPT-135, were recorded on a Bruker 400 MHz spectrometer using $CDCl_3$ as the solvent. Chemical shifts (δ) are reported in parts per million (ppm), coupling constants (J) are expressed in Hertz, and TMS serves as the internal standard. Mass-to-charge ratio (m/z) values were determined *via* High-Resolution Mass Spectrometry (HRMS) utilizing an Electrospray Ionization (ESI) source.

A 100 mL round-bottomed flask was charged with 2-chloro quinoline-3-carbaldehyde (**2**) (1 mmol, 1 eq.) and dissolved in 10 mL of Dimethyl Formamide (DMF). Subsequently, appropriate secondary amine heterocycles (morpholine, thiomorpholine, piperidine, and pyrrolidine) (2 mmol, 2 eq.) were added dropwise to the reaction mixture, followed by the addition of Potassium Carbonate, K_2CO_3 (2 mmol, 2 eq.). The reaction mixture was then refluxed for 3 hours at 80 °C, with the progression of the reaction monitored by Thin Layer Chromatography (TLC). Upon completion of the reaction, the organic phase was extracted using ethyl acetate. The organic extract was washed with a brine solution and subsequently filtered through anhydrous Na_2SO_4 to remove any residual moisture. The solvent was then removed under reduced pressure using a rotary evaporator. The resulting crude product was purified *via* column chromatography on silica gel, eluting with a solvent mixture of ethyl acetate/hexane (EtOH/Hexane) (8 : 2) to afford the pure compound (**3–6**).

3.2 Standard protocol for the synthesis of compounds (12–16)

In a 100 mL round-bottom flask, appropriate 2-amino benzophenone derivatives (**7–11**) (1 mmol, 1 eq.) were dissolved in 10 mL of ethanol. Acetylacetone (4 mmol, 4 eq.) was subsequently added dropwise to the reaction mixture. A few drops of concentrated hydrochloric acid (conc. HCl) were introduced at 0 °C. Then the reaction temperature was raised to 70 °C and refluxed for six hours. Progress of the reaction was monitored using Thin Layer Chromatography (TLC). Upon cooling, the reaction mixture was poured into cold water to precipitate yellow to off-white solids, which were then filtered under suction, dried, and subjected to recrystallization from ethanol to afford pure compounds (**12–16**).

3.3 Standard protocol for the synthesis of bis-quinolin-3-yl chalcones (17–36)

A mixture of respective compounds (**3–6**) (1 mmol, 1 eq.) and compounds (**12–16**) (1 mmol, 1 eq.), dissolved in ethanol (10 mL), was prepared in a reaction vessel equipped with a magnetic stir bar. Then the two pellets of sodium hydroxide (NaOH) were added and subsequently, the reaction mixture was stirred for six to eight hours at room temperature under irradiation with a 7 W Blue LED light source, kept at 2.0 cm away from the reaction vessel. The progress of the reaction was monitored using Thin Layer Chromatography (TLC) throughout the reaction duration. Upon completion of the reaction, observation of a bright yellow single spot on the TLC plate confirmed the full conversion of starting materials. The reaction mixture was then poured into cooled water, resulting in the precipitation of a yellow to orange-colored precipitate. After filtration, the precipitate was washed with cold water and dried. After being filtered out, the residue was washed with cold water and dried. Then the desired bis-quinolin-3-yl chalcones (**17–36**) were obtained by column chromatography with the solvent mixture of EtOAc/Hexane 8 : 2 and recrystallized using dichloromethane and methanol.

3.4 Photophysical characterisation

Using a spectrophotometer (SHIMADZU, model UV-1800) and a fluorometer (HITACHI, model F-7000), the absorption and emission spectra of the synthesized compounds were recorded using quartz cells with a 1 cm path length at room temperature. All the synthesized bis-quinolin-3-yl chalcones were dissolved in spectroscopic grade solvents of varying polarity, including petroleum ether, toluene, diethyl ether, dichloromethane, ethyl acetate, methanol, ethanol, acetonitrile, dimethylformamide, and dimethyl sulfoxide at a concentration of 2×10^{-5} mol L^{-1}. All the solutions were readily prepared at the time of the experiment, and it is seen that no aggregation formation occurs at the mentioned concentration. The resulting absorption spectra were utilised to investigate the solvatochromic effects

on the compounds. By using the comparison method, the emission quantum yield (Φ) of the compounds in acetonitrile was calculated using the following eqn (1),[62–64]

$$\varphi_S = \varphi_R \times \frac{(A_S \times Abs_R \times n_S^2)}{(A_R \times Abs_S \times n_R^2)} \quad (1)$$

where, φ_S = quantum yield of the sample, φ_R = quantum yield of the reference, A_S = integrated area under fluorescence curve of the sample, A_R = integrated area under the fluorescence curve of the reference, Abs_S = absorbance of the sample in the respective solution at an excitation wavelength, Abs_R = absorbance of the reference in the respective solution at the excitation wavelength, n_S = refractive index of sample, n_R = refractive index of reference. It is noted that methylene blue is used as a standard ($\varphi_R = 0.52$ in chloroform).[65,66]

3.5 Computational methods

The computational calculations of the series of novel bis-quinolin-3-yl chalcones were performed using the Gaussian 16W package and the Gauss view 6.1 program with density functional theory, DFT. Becke's hybrid exchange functional called "B3", combined with the LYP correlation functional, is the most widely applied of the many possible choices of exchange and correlation functionals. This is called the B3LYP method.[67] Thus, the geometry of all the synthesized compounds was optimized with the use of the B3LYP functionals and the 6-31G(d) basis set.[68] The basis set 631-G(d) is relatively good for energy determinations, and a heavy atom polarization term, d, was included to improve the energy output for large atoms.[69] Furthermore, the frontier molecular orbital features, the highest occupied molecular orbital (HOMO), and the lowest unoccupied molecular orbital (LUMO) were computed at the same energy level. Furthermore, the ionization potential (I), electron affinity (A),[70] electronegativity (χ), chemical hardness (η), chemical softness (σ), electrophilicity index (ω), nucleophilicity (ε), electron-accepting capacity (ω^+), electron-donating power (ω^-) are also calculated following Koopmans theorem.

4. Conclusion

A new series of bis-quinolin-3-yl chalcones were synthesized successfully by a novel, simple, and straightforward strategy of Claisen–Schmidt condensation under visible light irradiation. The present protocol provides fringe benefits over the traditional method without the use of any additional thermal energy. Moreover, this research sheds light on the relationship between molecular structure and optical properties of the synthesised chalcones. Through a comprehensive investigation encompassing solvatochromism studies, UV-visible absorption spectroscopy, and fluorescence analysis, we have elucidated key factors influencing the absorption and emission behaviour of these compounds. Our findings highlight the significance of solvent polarity, substituent effects, and molecular conformation on the observed spectral shifts and intensity changes. Particularly, compounds **18**, **23**, **28**, and **33** have good stability as well as good fluorescence intensity whereas compounds such as **21**, **26**, **31**, and **36** have less stability owing to the presence of an electron withdrawing group. Overall, this study contributes to the fundamental understanding of all compounds, with potential implications for developing novel photonic materials and applications.

Data availability

The data supporting this article have been included as part of the ESI.†

Author contributions

Conceptualization: IC; data curation: IC; investigation: IC; methodology: IC; supervision: SS; writing – original: IC; writing – review & editing: SS.

Conflicts of interest

There are no conflicts to declare.

Acknowledgements

The authors of this paper are very much thankful to the administration, of VIT, Vellore, India for providing the facilities to conduct the research work, for the seed grant SG20230087 and they are also appreciative of SIF-Chemistry for providing the NMR facility. The HRMS facility was also provided by the Chemistry department, at VIT, Vellore, for which the authors are grateful. Also, we would like to thank Dr V. Vijaykumar, professor, of VIT Vellore, for his valuable guidance.

Notes and references

1 H. Baig, R. Irfan, A. Rasool, S. Z. Hussain, S. A. Siddique, J. Iqbal, M. Alazmi, N. Alshammari, A. Alazmi, A. AlGhadhban, A. M. E. Sulieman, K. B. Said, H. ur Rehman and R. S. Z. Saleem, *J. Photochem. Photobiol., A*, 2024, **174**, 108173.
2 N. K. Sahu, S. S. Balbhadra, J. Choudhary and D. V. Kohli, *Curr. Med. Chem.*, 2012, **19**, 209.
3 Y. Xue, Y. Liu, L. An, L. Zhang, Y. Yuan, J. Mou, L. Liu and Y. Zheng, *Comput. Theor. Chem.*, 2011, **965**, 146.
4 R. K. S. Ahmad, S. D. Kulkarni, P. Melroy Lewis, P. Bhat and N. S. Shetty, *J. Photochem. Photobiol., A*, 2023, **437**, 114494.
5 H. Baig, A. Iqbal, A. Rasool, S. Z. Hussain, J. Iqbal, M. Alazmi, N. Alshammari, A. Alazmi, A. AlGhadhban, A. M. E. Sulieman, K. B. Said, H. U. Rehman and R. S. Z. Saleem, *ACS Omega*, 2023, **8**, 28499.
6 C. Y. Yang, M. Y. Lee, Y. L. Chen, J. P. Shiau, Y. H. Tsai, C. N. Yang, H. W. Chang and C. H. Tseng, *Int. J. Mol. Sci.*, 2023, **24**(7), 6034.
7 J. Aucamp and D. D. N'Da, *Exp. Parasitol.*, 2022, **236–237**, 108249.
8 M. Sharma, V. Chaturvedi, Y. K. Manju, S. Bhatnagar, K. Srivastava, S. K. Puri and P. M. S. Chauhan, *Eur. J. Med. Chem.*, 2009, **44**, 2081.

9 R. Abonia, D. Insuasty, J. Castillo, B. Insuasty, J. Quiroga, M. Nogueras and J. Cobo, *Eur. J. Med. Chem.*, 2012, **57**, 29.
10 M. Ibrahim-Ouali and F. Dumur, *Eur. Polym. J.*, 2021, **158**, 110688.
11 M. M. Makhlouf, A. S. Radwan and B. Ghazal, *Appl. Surf. Sci.*, 2018, **452**, 337.
12 H. Karaca and S. Kazancı, *J. Mol. Struct.*, 2022, **1248**, 131454.
13 P. Mahesha, N. S. Shetty and S. D. Kulkarni, *J. Fluoresc.*, 2022, **32**, 835.
14 S. Wangngae, K. Chansaenpak, J. Nootem, U. Ngivprom, S. Aryamueang, R. Y. Lai and A. Kamkaew, *Molecules*, 2021, **26**, 2979.
15 H. Liu, C. Guo, S. Guo, J. Fan, L. Wang and D. Shi, *Talanta*, 2019, **201**, 301.
16 M. Shkir, P. S. Patil, M. Arora, S. AlFaify and H. Algarni, *Spectrochim. Acta, Part A*, 2017, **173**, 445.
17 N. A. M. Daud, Q. A. Wong, B. S. Ooi, C. K. Quah, F. D. Ramzi, Y.-F. Win and P. S. Patil, *Chem. Phys. Impact*, 2024, **8**, 100565.
18 S. Prabu, R. Nagalakshmi and P. Srinivasan, *Spectrochim. Acta, Part A*, 2013, **103**, 45.
19 S. L. Gaonkar and U. N. Vignesh, *Res. Chem. Intermed.*, 2017, **43**, 6043.
20 A. Rammohan, J. S. Reddy, G. Sravya, C. N. Rao and G. V. Zyryanov, *Environ. Chem. Lett.*, 2020, **18**, 433.
21 N. A. A. Elkanzi, H. Hrichi, R. A. Alolayan, W. Derafa, F. M. Zahou and R. B. Bakr, *ACS Omega*, 2022, **7**, 27769.
22 S. S. Mukhtar, N. M. Morsy, A. S. Hassan, T. S. Hafez, H. M. Hassaneen and F. M. Saleh, *Egypt. J. Chem.*, 2022, **65**(8), 379.
23 G. Rajendran, D. Bhanu, B. Aruchamy, P. Ramani, N. Pandurangan, K. N. Bobba, E. J. Oh, H. Y. Chung, P. Gangadaran and B. C. Ahn, *Pharmaceuticals*, 2022, **15**, 1250.
24 M. A. Shalaby, S. A. Rizk and A. M. Fahim, *Org. Biomol. Chem.*, 2023, **21**, 5317.
25 A. Sharma and A. Saraswat, *J. Indian Chem. Soc.*, 2021, **98**, 100028.
26 V. Tiwari, J. Meshram, P. Ali, J. Sheikh and U. Tripathi, *J. Enzyme Inhib. Med. Chem.*, 2011, **26**, 569.
27 N. C. Desai, B. Y. Patel and B. P. Dave, *Med. Chem. Res.*, 2017, **26**, 109.
28 N. A. Peerzade, S. Y. Jadhav and R. B. Bhosale, *Asian J. Chem.*, 2020, **32**, 959.
29 R. Kachadourian, B. J. Day, S. Pugazhenti, C. C. Franklin, E. Genoux-Bastide, G. Mahaffey, C. Gauthier, A. Di Pietro and A. Boumendjel, *J. Med. Chem.*, 2012, **55**, 1382.
30 C. S. Cho, N. Y. Lee, T.-J. Kim and S. C. Shim, *J. Heterocycl. Chem.*, 2004, **41**, 409.
31 Y. Hemasri, *Heterocycl. Commun.*, 2009, **15**(6), 423.
32 M. Pradeep, M. Vishnuvardhan and T. Gangadhar, *Chem. Data Collect.*, 2023, **46**, 101020.
33 S. J. Deshpande, P. R. Leger and S. R. Sieck, *Tetrahedron Lett.*, 2012, **53**, 1772.
34 M. Rayees Ahmad, V. Girija Sastry, N. Bano and S. Anwar, *Arabian J. Chem.*, 2016, **9**, S931.
35 R. Prasath, P. Bhavana, S. Sarveswari, S. W. Ng and E. R. T. Tiekink, *J. Mol. Struct.*, 2015, **1081**, 201.
36 R. Prasath, P. Bhavana, S. W. Ng and E. R. T. Tiekink, *J. Organomet. Chem.*, 2013, **726**, 62.
37 E. Polo, N. Ibarra-Arellano, L. Prent-Peñaloza, A. Morales-Bayuelo, J. Henao, A. Galdámez and M. Gutiérrez, *Bioorg. Chem.*, 2019, **90**, 103034.
38 R. Prasath, P. Bhavana, S. Sarveswari, S. W. Ng and E. R. T. Tiekink, *J. Mol. Struct.*, 2015, **1081**, 201.
39 M. Pradeep, M. Vishnuvardhan and G. Thalari, *Chem. Data Collect.*, 2023, **46**, 101020.
40 K. Sun, Q. Y. Lv, X. L. Chen, L. B. Qu and B. Yu, *Green Chem.*, 2021, **23**, 232.
41 M. Tavakolian and M. Hosseini-Sarvari, *ACS Sustainable Chem. Eng.*, 2021, **9**, 4296.
42 J. R. Chen, X. Q. Hu, L. Q. Lu and W. J. Xiao, *Acc. Chem. Res.*, 2016, **49**, 1911.
43 M. H. Muhammad, X. L. Chen, Y. Liu, T. Shi, Y. Peng, L. Qu and B. Yu, *ACS Sustain. Chem. Eng.*, 2020, **8**, 2682.
44 P. Kumar, C. Joshi, A. K. Srivastava, P. Gupta, R. Boukherroub and S. L. Jain, *ACS Sustain. Chem. Eng.*, 2016, **4**, 69.
45 X. Ma, X. Chen, L. Ying, Y. Pang, Q. Zhong, D. Li and W. Sun, *Mol. Catal.*, 2023, **546**, 113276.
46 S. Fang and Y. H. Hu, *Chem. Soc. Rev.*, 2022, **51**, 3609.
47 D. Mateo, J. L. Cerrillo, S. Durini and J. Gascon, *Chem. Soc. Rev.*, 2021, **50**(3), 2173.
48 S. M. Ghouse, Y. S. Kumar, J. S. Jin, J. P. Kim, J. S. Bae, E. H. Chung, D. Y. Kim, E. K. Jang, F. R. Nawaz Khan and E. D. Jeong, *RSC Adv.*, 2014, **4**, 44408.
49 R. Prasath, S. Sarveswari, S. W. Ng and E. R. T. Tiekink, *Acta Crystallogr., Sect. E: Struct. Rep. Online*, 2013, **69**, o1414–o1415.
50 M. M. M. El-Miligy, M. E. Abdelaziz, S. M. Fahmy, T. M. Ibrahim, M. M. Abu-Serie, M. A. Mahran and A. A. Hazzaa, *J. Enzyme Inhib. Med. Chem.*, 2023, **38**(1), 2152810.
51 E. Srihari, G. S. Kumar, C. N. S. S. P. Kumar, R. K. Seth, S. Biswas, B. Sridhar and V. J. Rao, *Heterocycl. Commun.*, 2011, **17**, 111.
52 S. Pal, S. Durgadas, S. B. Nallapati, K. Mukkanti, R. Kapavarapu, C. L. T. Meda, K. V. L. Meda and M. Pal, *Bioorg. Med. Chem. Lett.*, 2011, **21**, 6573.
53 M. Gupta, *Bioorg. Med. Chem. Lett.*, 2011, **21**, 4919.
54 R. Ramesh, S. Ramesh, J. G. Malecki and A. Lalitha, *J. Iran. Chem. Soc.*, 2019, **16**, 1197.
55 D. Subhash and K. Bhaskar, *Russ. J. Org. Chem.*, 2020, **56**, 498.
56 G. C. Muscia, M. Bollini, J. P. Carnevale, A. M. Bruno and S. E. Asís, *Tetrahedron Lett.*, 2006, **47**, 8811.
57 N. D. Chavan and V. Vijayakumar, *RSC Adv.*, 2024, **14**, 21089.
58 S. Khopkar, M. Jachak and G. Shankarling, *Dyes Pigm.*, 2019, **161**, 1.
59 T. Zhang, Y. Xiao, H. Wang, S. Kong, R. Huang, V. Ka-Man Au, T. Yu and W. Huang, *Angew. Chem., Int. Ed.*, 2023, **62**, e202301896.
60 S. Sinha and D. Seth, *J. Mol. Liq.*, 2023, **388**, 122812.
61 M. Homocianu, *Microchem. J.*, 2024, **198**, 110166.

62 G. C. dos Santos, A. de Andrade Bartolomeu, V. F. Ximenes and L. C. da Silva-Filho, *J. Fluoresc.*, 2017, **27**, 271.
63 A. I. Martiryan, G. A. Shahinyan, I. L. Aleksanyan and L. P. Hambardzumyan, *J. Fluoresc.*, 2023, DOI: **10.1007/s10895-023-03519-2**.
64 R. Kumar, S. S. Acharya, P. Bhaumick, T. Parvin and L. H. Choudhury, *Tetrahedron*, 2023, **132**, 133250.
65 S. Khopkar, M. Jachak and G. Shankarling, *Spectrochim. Acta, Part A*, 2019, **211**, 114.
66 W. Li, L. Li, H. Xiao, R. Qi, Y. Huang, Z. Xie, X. Jing and H. Zhang, *RSC Adv.*, 2013, **3**, 13417.
67 *Advanced Organic Chemistry FIFTH EDITION Part A: Structure and Mechanisms*.
68 E. Polo, N. Ibarra-Arellano, L. Prent-Peñaloza, A. Morales-Bayuelo, J. Henao, A. Galdámez and M. Gutiérrez, *Bioorg. Chem.*, 2019, **90**, 103034.
69 O. C. Enudi, H. Louis, M. M. Edim, J. A. Agwupuye, F. O. Ekpen, E. A. Bisong and P. M. Utsu, *Heliyon*, 2021, **7**, e07531.
70 K. E. Roys and M. S L, *Opt. Mater.*, 2023, **145**, 114391.